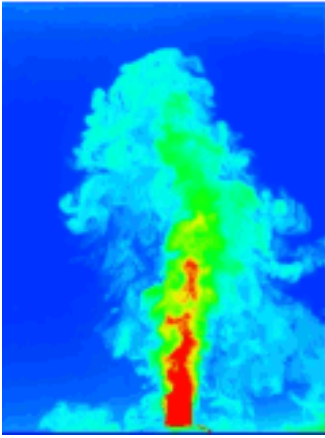


This article was downloaded by: [Tatiana Elizarova]

On: 05 August 2014, At: 05:16

Publisher: Taylor & Francis

Informa Ltd Registered in England and Wales Registered Number: 1072954 Registered office: Mortimer House, 37-41 Mortimer Street, London W1T 3JH, UK



Journal of Turbulence

Publication details, including instructions for authors and subscription information:

<http://www.tandfonline.com/loi/tjot20>

Simulation of laminar-turbulent transition in compressible Taylor-Green flow basing on quasi-gas dynamic equations

Ivan A. Shirokov^a & Tatiana G. Elizarova^b

^a Laboratory of Mathematical Modeling in Physics, Faculty of Computational Mathematics and Cybernetics, Moscow State University, Moscow, Russia

^b Keldysh Institute of Applied Mathematics, Russian Academy of Sciences, Russia

Published online: 25 Jul 2014.

To cite this article: Ivan A. Shirokov & Tatiana G. Elizarova (2014) Simulation of laminar-turbulent transition in compressible Taylor-Green flow basing on quasi-gas dynamic equations, Journal of Turbulence, 15:10, 707-730, DOI: [10.1080/14685248.2014.927581](https://doi.org/10.1080/14685248.2014.927581)

To link to this article: <http://dx.doi.org/10.1080/14685248.2014.927581>

PLEASE SCROLL DOWN FOR ARTICLE

Taylor & Francis makes every effort to ensure the accuracy of all the information (the "Content") contained in the publications on our platform. However, Taylor & Francis, our agents, and our licensors make no representations or warranties whatsoever as to the accuracy, completeness, or suitability for any purpose of the Content. Any opinions and views expressed in this publication are the opinions and views of the authors, and are not the views of or endorsed by Taylor & Francis. The accuracy of the Content should not be relied upon and should be independently verified with primary sources of information. Taylor and Francis shall not be liable for any losses, actions, claims, proceedings, demands, costs, expenses, damages, and other liabilities whatsoever or howsoever caused arising directly or indirectly in connection with, in relation to or arising out of the use of the Content.

This article may be used for research, teaching, and private study purposes. Any substantial or systematic reproduction, redistribution, reselling, loan, sub-licensing, systematic supply, or distribution in any form to anyone is expressly forbidden. Terms &

Conditions of access and use can be found at <http://www.tandfonline.com/page/terms-and-conditions>

Simulation of laminar–turbulent transition in compressible Taylor–Green flow basing on quasi-gas dynamic equations

Ivan A. Shirokov^{a*} and Tatiana G. Elizarova^b

^aLaboratory of Mathematical Modeling in Physics, Faculty of Computational Mathematics and Cybernetics, Moscow State University, Moscow, Russia; ^bKeldysh Institute of Applied Mathematics, Russian Academy of Sciences, Russia

(Received 26 March 2014; accepted 18 May 2014)

We report the results of numerical simulation of laminar–turbulent transition in the Taylor–Green vortex for viscous compressible gas flow basing on quasi-gas-dynamic (QGD) equations. Here the QGD system is obtained by a temporal averaging of the Navier–Stokes equations. The additional dissipative terms in QGD system serve to model the effects of the unresolved subgrid scales. Comparison with direct numerical simulation and large eddy simulation reference data demonstrates that QGD numerical algorithm provides a uniform and adequate simulation of both laminar and turbulent evolution of the vortex for Reynolds numbers from 100 up to 5000, including transition.

Keywords: laminar–turbulent transition; quasi-gas-dynamic equations; finite-difference scheme; Taylor–Green compressible flow; subgrid model

1. Introduction

The evolution of the single-vortex flow, defined at the initial time as the Taylor–Green vortex [1], may be one of the simplest flow for which a laminar–turbulent transition can be observed numerically. This process includes two stages. At the first stage, the large-scale vorticities break into smaller ones in laminar regime. Then, if the initial Reynolds number is large enough, after the time point corresponding to the maximum dissipation rate, the vortex decay leads to a turbulent energy cascade, which is interpreted as turbulence. Therefore, the Taylor–Green flow presents the transition into isotropic turbulence. For small Reynolds numbers, a vortex decays in a laminar regime. Taylor–Green flow has been well examined for both laminar and turbulent flows. Due to its relative numerical simplicity, it is used as a test case for numerical algorithms applied to turbulent flow simulations for incompressible flows or for the flows that are close to incompressible limit in direct numerical simulation (DNS) (e.g. [1–6]), large eddy simulation (LES) and implicit LES approaches [7–10].

Here we present the results of Taylor–Green vortex simulations based on the quasi-gas-dynamic (QGD) equation system for viscous compressible flows. The QGD system can be interpreted as the Navier–Stokes equation system averaged or smoothed, over some small time or space interval. The smoothing gives rise to the strongly nonlinear additional dissipation terms proportional to the small parameter τ . The first variants of the QGD system have been published more than three decades ago by Chetverushkin, Elizarova and Sheretov. From this time, the QGD system was widely used to construct numerical algorithms for gas flow simulations. The obtained results may be seen in [11–13], citations

*Corresponding author. Email: ivanshirokov@inbox.ru, ishirokov@cs.msu.su

herein (e.g. [14–16]), and in the recent papers. A number of theoretical results including exact solutions of QGD system and the close relations between QGD and Navier–Stokes systems have been established in [11]. A number of other theoretical results, including Petrovskii parabolicity and linearised stability of equilibrium solutions of QGD system, were analysed in e.g. [17,18].

QGD equations were created first for supersonic flow simulations, where additional dissipative τ -terms, adaptive to the flow parameters, stabilise numerical solutions in the shock-wave regions. Excellent capabilities of QGD algorithm in numerical simulation of supersonic gas flows were shown in e.g. [19] for 10 well-known test cases, consisting of different kinds of Riemann problems, including Sod, Noh and peak problems, and also the Woodward–Collela blast and Shu–Osher problems. In all cases, the QGD numerical solution monotonically converges to the reference data with a decreasing space step.

Later, it was noted that QGD equations open nice perspectives for the numerical simulation of turbulent flows. Here additional τ -dissipation may be regarded as an original form of subgrid dissipation, analogous to one used in LES or implicit LES method. Numerical simulations of flows in which shock waves and turbulence may coexist and interact dynamically are challenging tasks because of the contradictory requirements to numerical methods used to simulate turbulence and shock-wave phenomena [20].

The first encouraging QGD simulations of laminar–turbulent transition in a separated flow over a backward-facing step in two-dimensional (2D) formulation are presented in e.g. [21]. Several QGD calculations of this problem were repeated for 3D flows [22]. Three-dimensional laminar–turbulent boundary-layer transition in a hypersonic flow was observed in [23,24].

In the present paper, we examine the QGD system in calculations of the Taylor–Green vortex decay in nitrogen at a temperature of normal conditions. The variations of Reynolds number Re are achieved by variations of gas density and pressure. Numerical results are compared with reference data for laminar ($Re = 100$ and 280) and turbulent ($Re = 1600$ and 5000) vortex decay regimes, calculated in DNS and LES approaches. Computations were carried out on highly parallel computer K-100 [25].

In Section 2, the statement of the classical Taylor–Green vortex flow is presented. The development of QGD system and its relations with Navier–Stokes equations are discussed in Section 3. Section 4 briefly presents the numerical algorithm. Numerical results for $Re = 100$, 280 and 1600 are shown in Sections 5, 6 and 7. In Section 8, the symmetry properties of the QGD algorithm together with the computational results for nearly inviscid flow decay with $Re = 5000$ are collected. In Section 9, we state the further possibilities of the QGD scheme in compressible turbulent flow simulations.

2. Problem statement and flow conditions

According to [4], we examine a Taylor–Green vortex flow in a periodic square box as $-\pi L \leq x, y, z \leq \pi L$ in Cartesian coordinates. In our case, $\pi L = 0.016$ m. Working gas is nitrogen that is described by its density $\rho(x, y, z, t)$, velocity with components $u_x(x, y, z, t)$, $u_y(x, y, z, t)$, $u_z(x, y, z, t)$ and pressure $p(x, y, z, t)$. We also denote the velocity components as u_i . The same notation is used for all vector and tensor components below, if necessary.

The initial flow field for the Taylor–Green vortex is given by [1–7]

$$\begin{aligned} u_x &= U_0 \sin(x/L) \cos(y/L) \cos(z/L), \\ u_y &= -U_0 \cos(x/L) \sin(y/L) \cos(z/L), \end{aligned}$$

$$u_z = 0,$$

$$p = p_0 + \frac{\rho_0 U_0^2}{16} (\cos(2x/L) + \cos(2y/L)) (\cos(2z/L) + 2). \quad (1)$$

The initial temperature distribution is uniform in space: $T = T_0 = 273$ K. The initial density is governed by the equation of state for a perfect gas:

$$\rho = p/(RT). \quad (2)$$

The gas constant for nitrogen is $R = 297 \text{ J kg}^{-1} \text{ K}^{-1}$. Initial flow parameters ρ_0 , p_0 and T_0 are also connected by the state equation $p_0 = \rho_0 RT_0$.

We introduce a Mach number for the initial conditions

$$\text{Ma} = U_0/c_{s0} = 0.1, \quad (3)$$

where the speed of sound for nitrogen corresponding to the initial temperature is $c_{s0} = \sqrt{\gamma RT_0} = 337$ m/s, and the specific heat ratio is $\gamma = 7/5$ [26]. The Mach number used in calculations is small and the solution obtained for the velocity and pressure fields must be very close to those obtained assuming an incompressible flow.

We introduce the Reynolds number as

$$\text{Re} = \rho_0 U_0 L / \mu_0, \quad (4)$$

where $\mu_0 = 1.67 \times 10^{-5} \text{ kg/(m s)}$ is the dynamic shear viscosity for nitrogen at temperature $T_0 = 273$ K [26].

We calculate the flows with $\text{Re} = 100, 280$ and 1600 to compare the results with the reference data from [1–6], and $\text{Re} = 5000$ that is compared with data from [2] and [8]. The results of inviscid flow calculations of Taylor–Green vortex flow in LES approximation are presented in e.g. [7], using four high-order numerical methods, namely Jameson multi-stage scheme, Roe–TVD–MUSCL scheme and essentially non-oscillatory (ENO) schemes.

All our calculations are performed in dimensional values. In order to respect the desirable Re and Ma numbers, we define the initial values in the next order: at first, we define the initial velocity U_0 using Equation (3), density ρ_0 with Equation (4), pressure $p_0 = \rho_0 RT_0$, and then we define initial velocity and pressure distributions by Equation (1) and initial density field by Equation (2). The different values of the Reynolds number are obtained by adjusting the flow density and pressure for reference temperature.

The boundary conditions are taken as periodic in the three directions, which means that we assume a non-limited space containing a system of similar Taylor–Green vortices.

Some preliminary computational results for $\text{Re} = 100, 280$ and 1600 have been published in [27].

3. Quasi-gas-dynamic equation system

QGD equations are closely related to Navier–Stokes equations for viscous compressible gas flows and can be regarded as their generalisation [11–13]. It was shown [28] that QGD equations can be obtained by averaging Navier–Stokes equations over a small time interval, which results in additional smoothing or regularisation of the equation system. Below we present a brief description of this way to obtain QGD system basing on Navier–Stokes equations.

The viscous compressible Navier–Stokes equations [29,30] in the absence of external forces and heat sources can be presented in the following form:

$$\frac{\partial \rho}{\partial t} + \frac{\partial}{\partial x_i} J_i = 0, \quad (5)$$

$$\frac{\partial \rho u_i}{\partial t} + \frac{\partial}{\partial x_j} J_j u_i + \frac{\partial}{\partial x_i} p = \frac{\partial}{\partial x_j} \Pi_{NSji}, \quad (6)$$

$$\frac{\partial}{\partial t} \rho \left(\frac{u^2}{2} + \varepsilon \right) + \frac{\partial}{\partial x_i} J_i \left(\frac{u^2}{2} + \varepsilon + \frac{p}{\rho} \right) + \frac{\partial}{\partial x_i} q_{NSi} = \frac{\partial}{\partial x_i} \Pi_{NSij} u_j. \quad (7)$$

Here,

$$J_i = \rho u_i \quad (8)$$

denotes a mass flux vector, and $u^2 = u_x^2 + u_y^2 + u_z^2$. System (5)–(7) is supplemented with the equation of state (2) for the perfect gas and with the following expressions for the viscous stress tensor and the heat flux vector:

$$\Pi_{NSij} = \mu \left(\frac{\partial}{\partial x_i} u_j + \frac{\partial}{\partial x_j} u_i - \frac{2}{3} \delta_{ij} \frac{\partial}{\partial x_k} u_k \right) + \xi \delta_{ij} \frac{\partial}{\partial x_k} u_k, \quad q_{NSi} = -k \frac{\partial}{\partial x_i} T, \quad (9)$$

where the indices i and j denote coordinates x , y and z . The unknown values in system (5)–(7) are the density ρ , the velocity components u_i and the internal energy ε . The coefficients of the dynamic viscosity μ , volume viscosity ξ and the thermal conductivity k are positive, and δ_{ij} is the Kronecker delta.

To obtain the QGD equation system, let us average the equation system (5)–(7) over a small time interval Δt . We assume that Δt is sufficiently small and does not exceed the characteristic hydrodynamic time-space scale of the problem under consideration. Therefore, the equation system obtained will imply only averaged gas-dynamic parameters, and will not depend on the details of the unresolved scales of the order of $\sim \Delta t$ and $\sim \Delta t c_s$.

We calculate the time integrals accordingly with [28] in approximate form as

$$\frac{1}{\Delta t} \int_t^{t+\Delta t} f(x_i, t') dt' \approx f(x_i, t) + \tau \frac{\partial f(x_i, t)}{\partial t}, \quad (10)$$

where f denotes the averaged gas-dynamic parameters ρ , p , ε and u_i . The smoothing parameter τ is related to interval of time averaging ($0 \leq \tau \leq \Delta t$) and can be considered as a small free parameter that will be defined later.

Introducing the relation (10) in Equations (5)–(7), we restrict our consideration only by the first-order terms and neglect the terms of the order $O(\tau^2)$, $O(\tau\mu)$ and $O(\tau k)$. We omit terms of the form $(\frac{\partial}{\partial t} \tau \frac{\partial}{\partial t})$ while computing the time derivatives, supposing that they are small compared with the first-order time derivatives. So we find that averaged system becomes

$$\frac{\partial \rho}{\partial t} + \frac{\partial}{\partial x_i} \left(\rho u_i + \tau \frac{\partial}{\partial t} \rho u_i \right) = 0, \quad (11)$$

$$\frac{\partial \rho u_i}{\partial t} + \frac{\partial}{\partial x_j} \left[\left(\rho u_j + \tau \frac{\partial}{\partial t} \rho u_j \right) u_i + \tau \rho u_j \frac{\partial}{\partial t} u_i \right] + \frac{\partial}{\partial x_i} \left(p + \tau \frac{\partial}{\partial t} p \right) = \frac{\partial}{\partial x_j} \Pi_{NSji}, \quad (12)$$

$$\frac{\partial}{\partial t} \rho \left(\frac{u^2}{2} + \varepsilon \right) + \frac{\partial}{\partial x_i} \left[\left(\rho u_i + \tau \frac{\partial}{\partial t} \rho u_i \right) \left(\frac{u^2}{2} + \varepsilon + \frac{p}{\rho} \right) + \tau \rho u_i \left(u_j \frac{\partial}{\partial t} u_j + \frac{\partial \varepsilon}{\partial t} + p \frac{\partial}{\partial t} \frac{1}{\rho} + \frac{1}{\rho} \frac{\partial p}{\partial t} \right) \right] + \frac{\partial}{\partial x_i} q_{NSi} = \frac{\partial}{\partial x_i} \Pi_{NSij} u_j. \quad (13)$$

The next step consists of the calculation of the τ -terms with time derivatives and transformation of the obtained system to the flux form similar to the Navier–Stokes system (5)–(7).

Continuity Equation (11) is transformed as follows. We find the time derivative from the Euler momentum equation as

$$\frac{\partial \rho u_i}{\partial t} = - \frac{\partial}{\partial x_j} \rho u_j u_i - \frac{\partial}{\partial x_i} p. \quad (14)$$

Substituting this expression into Equation (11) yields

$$\frac{\partial \rho}{\partial t} + \frac{\partial}{\partial x_i} \left[\rho u_i - \tau \left(\frac{\partial}{\partial x_j} \rho u_j u_i + \frac{\partial}{\partial x_i} p \right) \right] = 0. \quad (15)$$

Introducing the notation

$$w_i = \frac{\tau}{\rho} \left(\frac{\partial}{\partial x_j} \rho u_j u_i + \frac{\partial}{\partial x_i} p \right), \quad J_i = \rho(u_i - w_i), \quad (16)$$

we obtain the following time-averaged, or smoothed, continuity equation:

$$\frac{\partial \rho}{\partial t} + \frac{\partial}{\partial x_i} J_i = 0, \quad (17)$$

where J_i denotes the mass flux vector that differs from the Navier–Stokes mass flux vector ρu_i (8) by the strongly nonlinear values proportional to the small parameter τ .

To transform the momentum and energy equations, we use the Euler equations and differential identities following from them. For an ideal polytropic gas with the equations of state,

$$p = \rho RT, \quad \varepsilon = \frac{RT}{\gamma - 1}, \quad (18)$$

these identities can be written as

$$\frac{\partial}{\partial t} \frac{1}{\rho} + u_i \frac{\partial}{\partial x_i} \frac{1}{\rho} - \frac{1}{\rho} \frac{\partial}{\partial x_i} u_i = 0, \quad (19)$$

$$\frac{\partial}{\partial t} u_i + u_j \frac{\partial}{\partial x_j} u_i + \frac{1}{\rho} \frac{\partial}{\partial x_i} p = 0, \quad (20)$$

$$\frac{\partial}{\partial t} \varepsilon + u_i \frac{\partial}{\partial x_i} \varepsilon + \frac{p}{\rho} \frac{\partial}{\partial x_i} u_i = 0, \quad (21)$$

$$\frac{\partial}{\partial t} p + u_i \frac{\partial}{\partial x_i} p + \gamma p \frac{\partial}{\partial x_i} u_i = 0. \quad (22)$$

The analogous transformation of the momentum equation (12) is done in the next form. Using Equation (16) and identities (20) and (22), we obtain

$$\begin{aligned} \frac{\partial \rho u_i}{\partial t} + \frac{\partial}{\partial x_j} \left[(\rho u_j - \rho w_j) u_i + \tau \rho u_j \left(-u_k \frac{\partial}{\partial x_k} u_i - \frac{1}{\rho} \frac{\partial}{\partial x_i} p \right) \right] \\ + \frac{\partial}{\partial x_i} \left[p + \tau \left(-u_k \frac{\partial}{\partial x_k} p - \gamma p \frac{\partial}{\partial x_k} u_k \right) \right] = \frac{\partial}{\partial x_j} \Pi_{NSji}. \end{aligned} \quad (23)$$

Thus, the smoothed momentum equation is written as

$$\frac{\partial \rho u_i}{\partial t} + \frac{\partial}{\partial x_j} J_j u_i + \frac{\partial}{\partial x_i} p = \frac{\partial}{\partial x_j} \Pi_{ji}, \quad (24)$$

where the viscous stress tensor is given by

$$\Pi_{ji} = \Pi_{NSji} + \tau \rho u_j \left(u_k \frac{\partial}{\partial x_k} u_i + \frac{1}{\rho} \frac{\partial}{\partial x_i} p \right) + \tau \delta_{ji} \left(u_k \frac{\partial}{\partial x_k} p + \gamma p \frac{\partial}{\partial x_k} u_k \right). \quad (25)$$

To transform the total energy balance equation (13), we use all four Euler identities (19)–(22). As a result, we get

$$\begin{aligned} \frac{\partial}{\partial t} \rho \left(\frac{u^2}{2} + \varepsilon \right) + \frac{\partial}{\partial x_i} J_i \left(\frac{u^2}{2} + \varepsilon + \frac{p}{\rho} \right) + \frac{\partial}{\partial x_i} \tau \rho u_i u_j \left(-u_k \frac{\partial}{\partial x_k} u_j - \frac{1}{\rho} \frac{\partial p}{\partial x_j} \right) \\ - \frac{\partial}{\partial x_i} \tau \rho u_i \frac{1}{\rho} \left(u_k \frac{\partial}{\partial x_k} p + \gamma p \frac{\partial}{\partial x_j} u_j \right) + \frac{\partial}{\partial x_i} \tau \rho u_i \left(-u_k \frac{\partial}{\partial x_k} \varepsilon - \frac{p}{\rho} \frac{\partial}{\partial x_k} u_k \right) \\ + \frac{\partial}{\partial x_i} \tau \rho u_i p \left(-u_k \frac{\partial}{\partial x_k} \frac{1}{\rho} + \frac{1}{\rho} \frac{\partial}{\partial x_k} u_k \right) + \frac{\partial}{\partial x_i} q_{NSi} = \frac{\partial}{\partial x_i} \Pi_{NSij} u_j. \end{aligned} \quad (26)$$

Combining like terms gives the following time-averaged total energy equation:

$$\frac{\partial}{\partial t} \rho \left(\frac{u^2}{2} + \varepsilon \right) + \frac{\partial}{\partial x_i} J_i \left(\frac{u^2}{2} + \varepsilon + \frac{p}{\rho} \right) + \frac{\partial}{\partial x_i} q_i = \frac{\partial}{\partial x_i} \Pi_{ij} u_j. \quad (27)$$

where the heat flux is given by

$$q_i = q_{NSi} - \tau \rho u_i \left(u_k \frac{\partial}{\partial x_k} \varepsilon + p u_j \frac{\partial}{\partial x_j} \frac{1}{\rho} \right). \quad (28)$$

The time-averaged angular momentum balance equation is derived in a similar fashion and coincides with the equation obtained in [11] as an exact consequence of the QGD momentum balance equation (24). Therefore, the QGD equation system presented here does not disturb the angular moment balance of the gas-dynamic system.

For the QGD system, the entropy balance equation with non-negative dissipation function Φ was obtained:

$$\begin{aligned} \Phi = & \frac{\Pi_{\text{NS}} : \Pi_{\text{NS}}}{2\mu} + \frac{p\tau}{\rho^2} \left(\frac{\partial}{\partial x_i} \rho u_i \right)^2 + \tau\rho \left(u_k \frac{\partial}{\partial x_k} u_i + \frac{1}{\rho} \frac{\partial}{\partial x_i} p \right)^2 \\ & + \frac{\tau\rho}{\varepsilon} \left(u_i \frac{\partial}{\partial x_i} \varepsilon + \frac{p}{\rho} \frac{\partial}{\partial x_i} u_i \right)^2. \end{aligned} \quad (29)$$

The τ -terms bring an additional non-negative entropy production and thus they have a dissipative character [11,13].

The additional strongly nonlinear τ -terms that appear due to averaging are second-order space derivatives in factor of a small parameter τ that has the dimension of time. For $\tau = 0$, the QGD equation system reduces to the classical system (5)–(7). The influence of additional τ -terms is different for the quasi-stationary and strong non-stationary flows. According to [11,13], for slowly variable laminar flows, τ -terms have the order $O(\tau^2)$ and influence only the accuracy of the solution. However, for rapidly variable turbulent flows, τ -terms have the order of $O(\tau)$ and can bring a considerable contribution to the solution.

In the gas flow calculations, τ -terms work as efficient adaptive dissipation, which improve the stability of the numerical solution in the regions with strong variations of parameters, as shock wave and boundary regions, and at the same time, vanish in the regions with smooth solution.

At the same time, τ -terms can be regarded as a form of subgrid dissipation, which smooth the unresolved time-space scales. The QGD τ -terms are more complex and differ from the tradition approach to calculate turbulent flows. In LES and RANS approaches, viscosity coefficient μ is replaced by $\mu + \mu_t$, where μ_t is the turbulent viscosity. The last one can be estimated by Boussinesq–Prandtl hypothesis [29] as $\mu_t \sim \rho u' l$ with u' as the velocity fluctuations and l as the turbulent mixing length. This form of turbulent viscosity is included in τ terms, added to Π_{NS} (25), for example,

$$\Pi_{yx} \sim \mu \frac{\partial u_x}{\partial y} + \tau u_y \rho u_y \frac{\partial u_x}{\partial y} = (\mu + \mu_t) \frac{\partial u_x}{\partial y},$$

where $\mu_t = \tau u_y^2 \rho = \rho u_y l$, with $l = \tau u_y$.

Compared with RANS or LES models, dissipative τ -terms appear not only in the momentum and energy equations, but also in the continuity equation. This simulates the turbulent mass diffusion, which is inherent to turbulent mixing. In this sense, τ -smoothing correlates with implicit LES methods (e.g. [9,10]), where cell-averaging discretisation of the flow variables acts as an implicit filter for all equations of the system [31].

Near a wall, both pressure gradient and velocity components are small and all τ -terms vanish. In the limiting case of $\text{Re} \rightarrow \infty$ QGD system as the Navier–Stokes one takes the form of Prandtl equations.

The generalisation of the QGD system for the flows with external forces and heat sources was done in [11,13]. Flows with a generalised equation of state may be described by QGD equations in the form of [32]. QGD algorithm for shallow-water flows is presented in e.g. [33].

4. Governing equations and numerical algorithm

Numerical algorithm is based on the QGD equations presented in the flux form:

$$\frac{\partial \rho}{\partial t} + \frac{\partial}{\partial x_\alpha} J_\alpha = 0 \quad (30)$$

$$\frac{\partial \rho u_\alpha}{\partial t} + \frac{\partial}{\partial x_\beta} J_\beta u_\alpha + \frac{\partial}{\partial x_\alpha} p = \frac{\partial}{\partial x_\beta} \Pi_{\beta\alpha} \quad (31)$$

$$\frac{\partial}{\partial t} E + \frac{\partial}{\partial x_\alpha} J_\alpha H + \frac{\partial}{\partial x_\alpha} q_\alpha = \frac{\partial}{\partial x_\alpha} \Pi_{\alpha\beta} u_\beta \quad (32)$$

for ideal polytropic gas (18) with closing relations (16), (25) and (28). Here E and H are the total energy per unit volume and total specific enthalpy, respectively,

$$E = \rho \left(\frac{u^2}{2} + \varepsilon \right), \quad H = \left(\frac{u^2}{2} + \varepsilon + \frac{p}{\rho} \right) = \frac{E + p}{\rho}.$$

The heat conductivity coefficient is given by

$$k = \frac{\mu \gamma R}{\text{Pr}(\gamma - 1)}, \quad (33)$$

where Pr is the Prandtl number. In our consideration, $\text{Pr} = 0.71$ according to [4].

The gas viscosity coefficient μ , appearing in expressions for Π_{NS} and q_{NS} , is defined by a temperature power-law [26]:

$$\mu = \mu_0 \left(\frac{T}{T_0} \right)^\omega, \quad (34)$$

where ω -value is related to the intermolecular potential for gas molecules. For nitrogen, $\omega = 0.74$ [26]. Here the bulk, or volume, viscosity coefficient is supposed to be zero: $\xi = 0$ according to [4].

In the present applications, we define the relaxation parameter, appearing in formulas (9)–(12), as

$$\tau = \alpha \frac{h}{c_s}, \quad (35)$$

where $c_s = \sqrt{\gamma RT}$ is the sound velocity estimated locally and h is the grid resolution. In a low-supersonic flow, the value of τ defines the time required for a perturbation to travel across a grid cell. The τ -terms account for subgrid dissipation that averages the pulsations of gas-dynamic values over the time and grid steps. Thus, coefficient α is a tuning parameter that defines the level of subgrid dissipation. According to numerical practice, it ranges in the interval of $0 < \alpha \leq 1$. The coefficient α is the only tuning parameter of the QGD subgrid model.

Note that if we replace the step size h by the value of a mean free path λ , and set $\alpha = 1$, then τ -value (35) is equal to Maxwellian relaxation time $\tau_M = \mu/p$, obtained in kinetic theory for ideal polytropic gas (e.g. [26]). Calculations of the rarefied flows by QGD system with $\tau = \tau_M$ were done in e.g. [11,13,14].

The reference value of a mean free path [26] using the initial flow conditions has the following form:

$$\lambda_0 = \mu_0 / (\rho_0 \sqrt{2\pi RT_0} \Omega / 4),$$

where

$$\Omega = 30 / ((7 - 2\omega)(5 - 2\omega)).$$

For all the presented calculations, including the smallest Reynolds number, the condition $\lambda_0 \ll h$ is satisfied, where h is the grid resolution or computational space step. Really, for $Re = 100$ estimation gives $\lambda_0 = 6.2 \times 10^{-6}$ m, while in our calculations the smallest space step $h = 2.5 \cdot 10^{-4}$ m.

For the numerical simulation of the initial-boundary problems (30)–(32) with initial condition (1) in the computation domain $-\pi L \leq x, y, z \leq \pi L$, we introduce a uniform grid over space and time $\Omega_{x,y,z,t} = \omega_x \otimes \omega_y \otimes \omega_z \otimes \omega_t$, with $\omega_x = (x_i, i = 0, \dots, N + 1, x_i = hi)$, $\omega_y = (y_j, j = 0, \dots, N + 1, y_j = hj)$, $\omega_z = (z_k, k = 0, \dots, N + 1, z_k = hk)$, $\omega_t = (t_d, d = 0, \dots, N_t, t_d = \Delta t d)$. The number of time steps N_t is not determined in advance.

For all gas-dynamic values, depending on space coordinates and time, we introduce grid functions. For example, for density it stands as $\rho(i, j, k, d) = \rho(x_i, y_j, z_k, t_d)$. All other gas-dynamic grid values have a similar form. The dimensions of the grid functions are those of physical values.

We use the explicit-in-time finite-volume scheme with the approximation of all space derivatives by second-order central differences as

$$\left. \frac{\partial f}{\partial x} \right|_{i,j,k} = \frac{f_{i+1/2,j,k} - f_{i-1/2,j,k}}{h}.$$

The gas-dynamic values with half integers are calculated with simple averaging by the adjacent cells, for example,

$$\rho_{i\pm 1/2,j,k} = 0.5(\rho_{i,j,k} + \rho_{i\pm 1,j,k}). \tag{36}$$

The time differences are approximated with first-order accuracy. The numerical algorithm is the same as in [11,13,21,23,34]. Explicit-time calculations directly describe the time evolution of the gas-dynamic flow. The convenient form of QGD system for finite-different approximation and programme coding is presented in [11,13].

The discrete form of Equation (30) can be written as

$$\begin{aligned} \rho_{i,j,k}^{d+1} = & \rho_{i,j,k} - \frac{\Delta t}{h} \left(J_{i+1/2,j,k}^x - J_{i-1/2,j,k}^x \right) - \frac{\Delta t}{h} \left(J_{i,j+1/2,k}^y - J_{i,j-1/2,k}^y \right) \\ & - \frac{\Delta t}{h} \left(J_{i,j,k+1/2}^z - J_{i,j,k-1/2}^z \right) \end{aligned} \tag{37}$$

Here, in the right-hand side of the equations, the index d is omitted and the coordinate indexes x, y, z are placed as $^x, ^y, ^z$. These relations mean that the change of the quantities inside a cell is defined by the fluxes through its boundaries. Half integer denotes the flux values on the interfaces between the cells.

For example, the x -component of the mass flux is approximated as

$$J_{i+1/2,j,k}^x = \rho_{i+1/2,j,k} (u_{i+1/2,j,k}^x - w_{i+1/2,j,k}^x), \quad (38)$$

where the space derivatives are calculated in a point $i + 1/2, j, k$ as

$$w_{i+1/2,j,k}^x = \frac{\tau}{\rho} \left(\frac{\partial \rho u_x^2}{\partial x} + \frac{\partial \rho u_x u_y}{\partial y} + \frac{\partial \rho u_x u_z}{\partial z} + \frac{\partial p}{\partial x} \right) \Big|_{i+1/2,j,k}. \quad (39)$$

It means that to compute the unknown ρ_{ijk}^{d+1} , the information from the adjacent points $(i \pm 1, j, k)$, $(i, j \pm 1, k)$ and $(i, j, k \pm 1)$ is required. The stencil of the scheme is a 3D cube that includes 27 space points.

Finite-volume analogues of Equations (31) and (32) are obtained by the same procedure.

The numerical algorithm is realised in the next way: at first, basing on the gas-dynamic values in the points (i, j, k) and $(i \pm 1, j \pm 1, k \pm 1)$ at the time step d , we determine the necessary gas-dynamic values in the half-integer points as e.g. Equation (38). Then, we calculate the fluxes (16, 25, 28) in the half-integer space points, then we calculate the values ρ , ρu_x , ρu_y , ρu_z and E in the next time step by the equations similar to Equation (37). The last step is the calculation of velocity components $u_i = \rho u_i / \rho$ and gas-dynamic temperature T using the state equation.

The periodic boundary conditions are realised by introducing shadow cells adjacent to a physical boundary. The gas-dynamic values at these cells are recalculated in each time layer. The boundary of the computational domain lies in the half-integer points (e.g. [13]).

The time step is determined by the Courant condition [13] as

$$\Delta t = \beta \frac{h}{c_{s0}}, \quad (40)$$

where β is the Courant number. The space step h is employed in the expression of relaxation parameter τ (14), and Courant number is directly related to the α -coefficient. In all calculations below, $\beta = 0.1$.

The QGD numerical scheme for non-uniform space grids could be constructed by replacing h for h_{xi} , h_{yj} and h_{zk} . Explicit QGD schemes for non-structured triangle grids are constructed and used in 2D calculations in [12,13,35].

As in [22,34], the calculations are performed in dimensional variables. For comparison with the reference data, we present the results of the calculations in dimensionless form using the reference parameters L , U_0 and ρ_0 . Therefore, the non-dimensional time is $t_{nd} = t/t_0$, where $t_0 = L/U_0 = 1.512 \times 10^{-4}$ s, and the non-dimensional value of kinetic energy per unit volume is $E_{nd} = E/(\rho_0 U_0^2)$.

The presented numerical algorithm is simple because of its explicit form and restricted space stencil. Only central-difference approximations are used and additional monotonisation or limiting functions are not required. Parallel realisation of the numerical method is natural and implies the domain-decomposition technique.

Results have been obtained on K-100 computer system [25] which was constructed in Keldysh Institute of Applied Mathematics, Russian Academy of Sciences, Moscow, Russia, in 2010. A parallel variant of the numerical algorithm was developed based on a decomposition of the computational domain by planes $x = \text{const}$. The message passing interface (MPI) was used. Our code is portable between multiprocessor systems that support the C language and MPI standard.

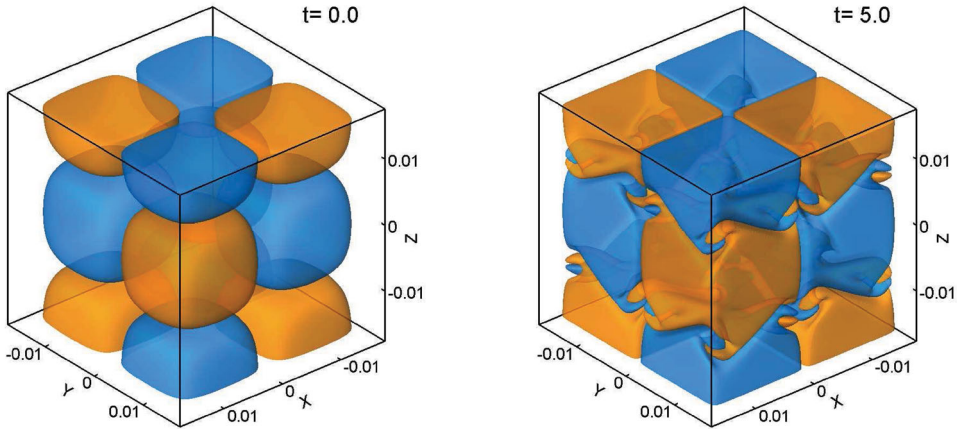


Figure 1. Evolution of iso-surfaces of z -component of vorticity for $Re = 100$, $t = 0.0$, and $t = 5.0$.

For example, calculations on the grid with 128^3 points up to non-dimensional time $t = 22.5$ with 32 processing nodes of K-100 (Intel Xeon X5670) take about 17 hours of the computing time.

5. Computational results for $Re = 100$

Figure 1 illustrates the evolution of iso-surfaces of z -component of the dimensionless vorticity:

$$V_z = \frac{\partial u_y}{\partial x} - \frac{\partial u_x}{\partial y}. \quad (41)$$

Here $Re = 100$, and yellow colour corresponds to $V_z = 0.2$, blue colour corresponds to $V_z = -0.2$. Iso-surfaces are presented for the sequence of dimensionless time moments $t = 0, 5, 10, 15, 20$ and 22.5 . The computational parameters are as follows: the number of the grid points is 128^3 , the space step is $h = 2.5 \times 10^{-4}$ m and $\alpha = 0.1$, Courant number $\beta = 0.1$, but it can be increased at least two times.

From Figures 1–3, one can see that the regular initial velocity distribution (1) (Figure 1 for $t = 0$) breaks down into smaller structures, and later, these small-scale structures clearly retain the features of the initial anisotropy of Taylor–Green vortex. Further, the vortex flow dies out due to viscosity. Note that the dimensionless time interval $\Delta t = 1$ corresponds to the period of rotation of the initial vortex (1). The analysis of the constant gas-dynamic values shows that the symmetry of the flow is perfectly conserved, namely, with the accuracy of the computations.

Figure 4 (left) shows the temporal evolution of the decaying kinetic energy E_{kin} averaged over the calculation domain V_0 :

$$E_{kin} = \frac{1}{\rho_0 U_0^2 V_0} \int_{V_0} \frac{1}{2} \rho (u_x^2 + u_y^2 + u_z^2) dx dy dz. \quad (42)$$

Kinetic energy and time are represented in dimensionless form. The presented lines correspond to calculations with the number of grid points equal to 32^3 , 64^3 and 128^3 ,

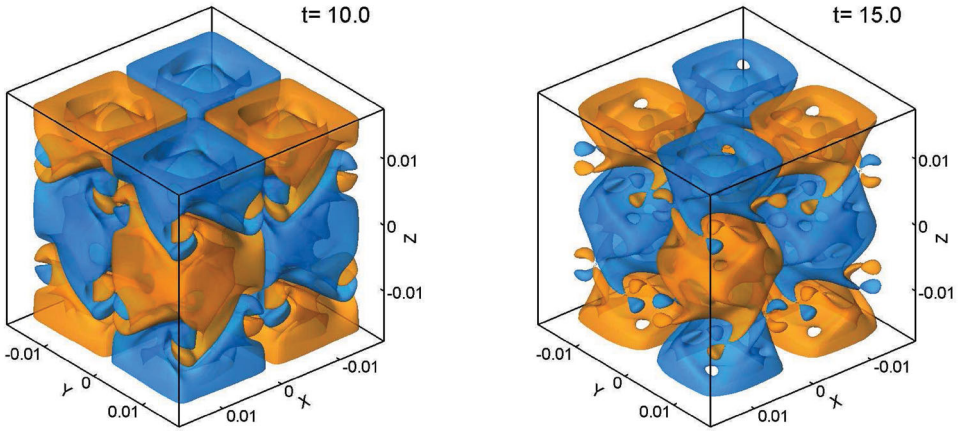


Figure 2. Evolution of iso-surfaces of z -component of vorticity for $Re = 100$, $t = 10.0$, and $t = 15.0$.

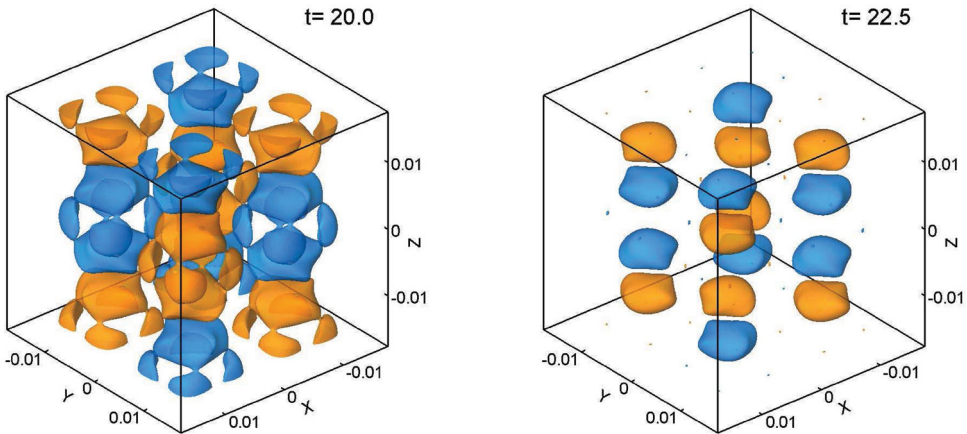


Figure 3. Evolution of iso-surfaces of z -component of vorticity for $Re = 100$, $t = 20.0$, and $t = 22.5$.

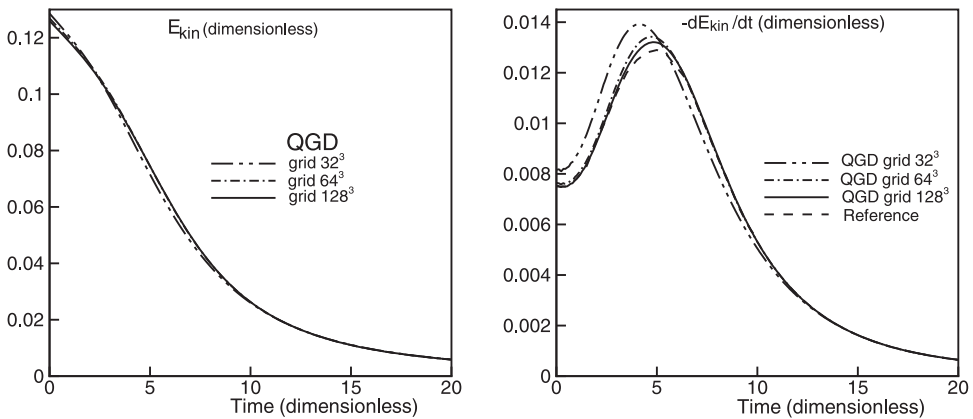


Figure 4. Grid convergence of kinetic energy E_{kin} and dissipation rate ϵ for $Re = 100$.

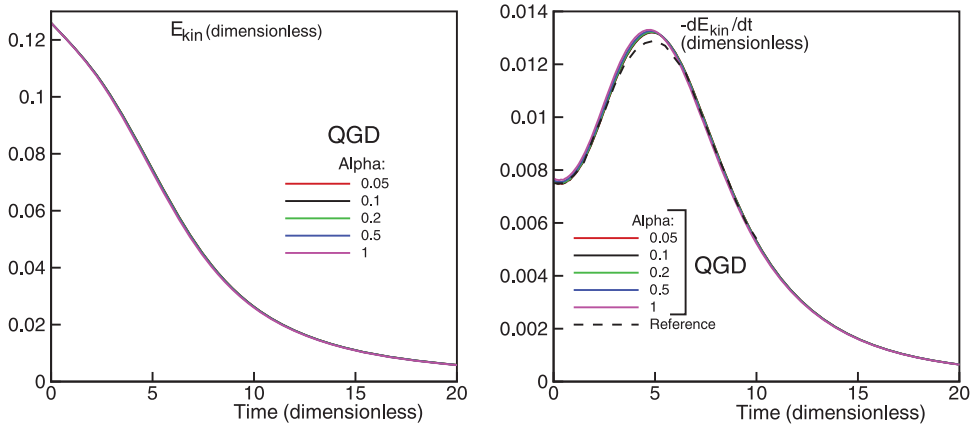


Figure 5. α -convergence of kinetic energy E_{kin} and dissipation rate ϵ for $Re = 100$.

and space steps equal to $h = 10^{-3}$, 5×10^{-4} m, and $h = 2.5 \times 10^{-4}$ m, for $\alpha = 0.1$.

Figure 4 (right) shows the temporal evolution of the dissipation rate $\epsilon = -dE_{kin}/dt$ together with the grid convergence for grid points 32^3 , 64^3 and 128^3 . The dashed line shows the reference data from Brachet et al. [1], obtained by different variants of discontinuous Galerkin method for incompressible flow. The figure shows that the evolutions of dissipation rate obtained for 64^3 and 128^3 points are in very good agreement with the reference results [1]. Maximal value of ϵ for $Re = 100$ is reached at dimensionless time $t_0 = 4.5$. This point distinguishes two different stages of Taylor–Green flow evolution: for $t < t_0$, the flow is laminar for all Reynolds numbers, and for $t > t_0$, the flow remains laminar for small Reynolds number and becomes turbulent with increasing Reynolds number [1]. For $t = t_0$, the Taylor–Green vortex flow is still well organised and anisotropic, thus the flow is laminar (see Figure 1). Furthermore, the flow pattern retains its initial anisotropy and remains laminar without generating the chaotic small vortex structures, typical for turbulent vortex decay. Therefore, the Taylor–Green vortex decay corresponds perfectly with results, reported in [1], for laminar flows with $Re < 500$.

For $Re = 100$, the variation of α -coefficient in the range $0.1 < \alpha < 1$ slightly changes the computational results (see Figure 5). Nevertheless, increasing of α allows to increase the Courant number proportionally. Strong decreasing of α can bring non-physical oscillations, and optimal α value is related with the desirable Courant number. These conclusions correspond with the practical experience of QGD calculation of laminar unsteady flows (e.g. [13]).

6. Computational results for $Re = 280$

Figures 6–8 illustrate the evolution of iso-surfaces of z -component of the dimensionless vorticity (41) for $Re = 280$. Here the number of the grid points is 128^3 , or $N = 128$, the space step is $h = 2.5 \times 10^{-4}$ m and $\alpha = 0.1$. Yellow colour corresponds to $V_z = 0.2$, and blue colour corresponds to $V_z = -0.2$. For comparison purposes, the time moments are the same as in Figures 1–3 for $Re = 100$.

Figure 9 shows the temporal evolution for kinetic energy E_{kin} (42) and its dissipation rate ϵ (right) for $Re = 280$. The dashed line refers to the reference data from

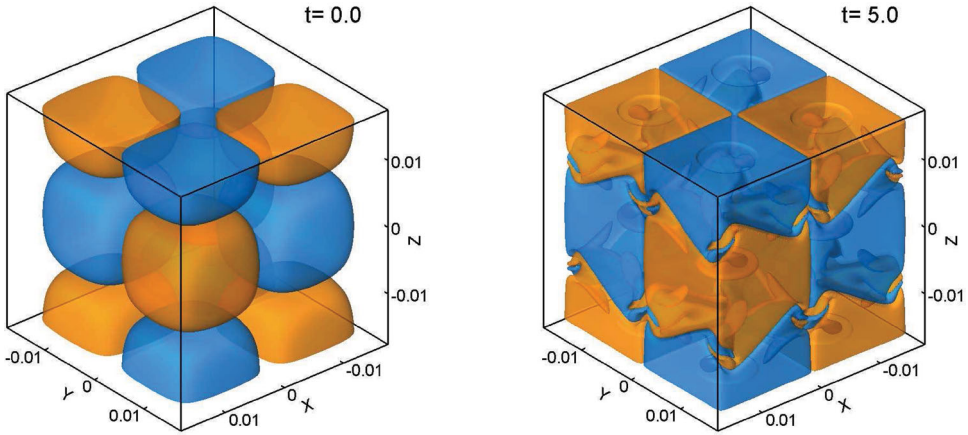


Figure 6. Evolution of iso-surfaces of z -component of vorticity for $Re = 280$, $t = 0.0$, and $t = 5.0$.

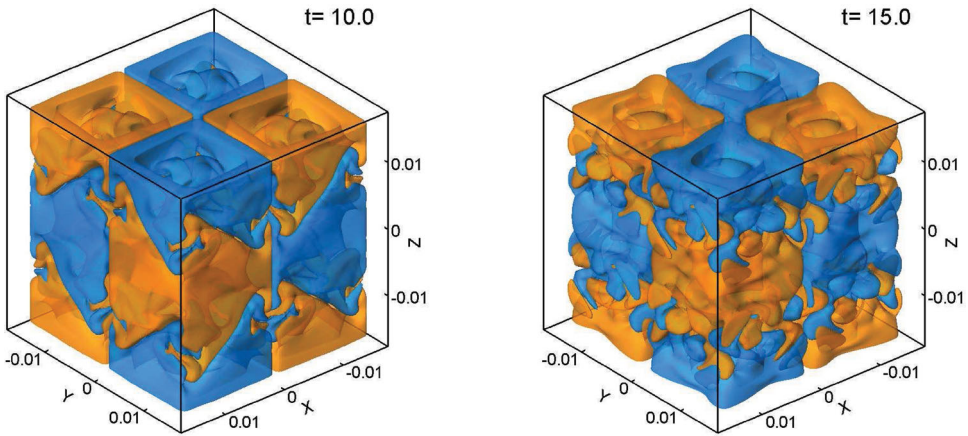


Figure 7. Evolution of iso-surfaces of z -component of vorticity for $Re = 280$, $t = 10.0$, and $t = 15.0$.

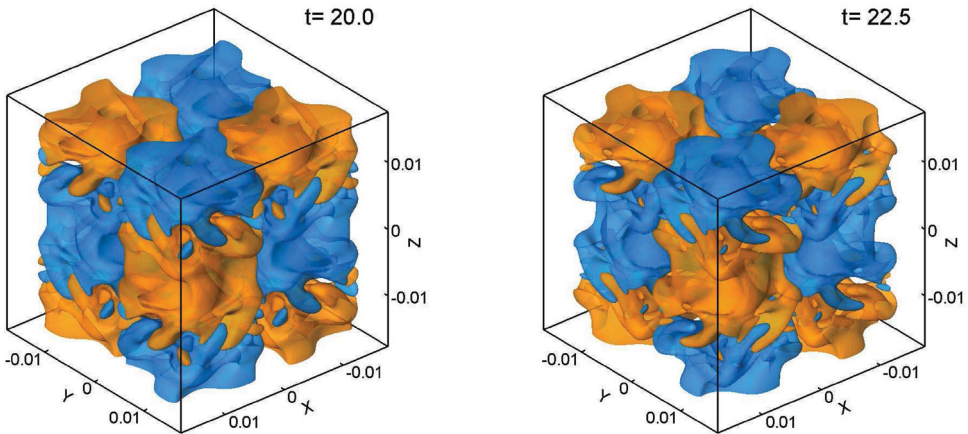


Figure 8. Evolution of iso-surfaces of z -component of vorticity for $Re = 280$, $t = 20.0$, and $t = 22.5$.

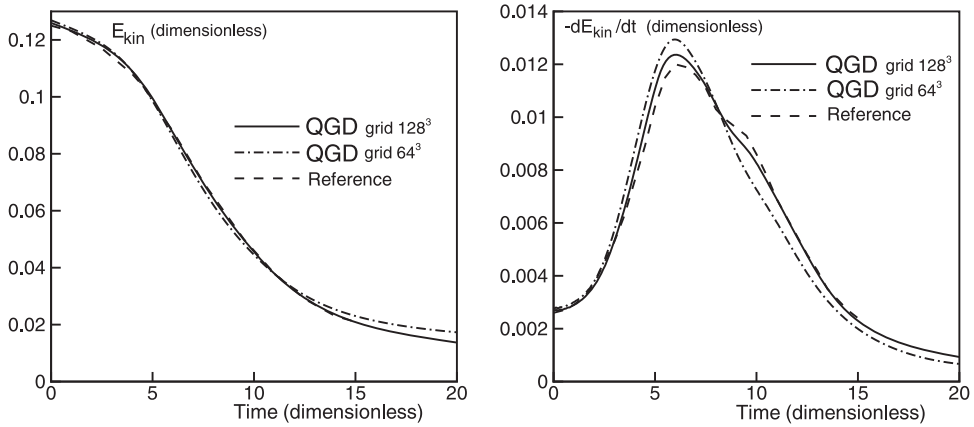


Figure 9. Grid convergence of kinetic energy E_{kin} and dissipation rate ϵ for $Re = 280$.

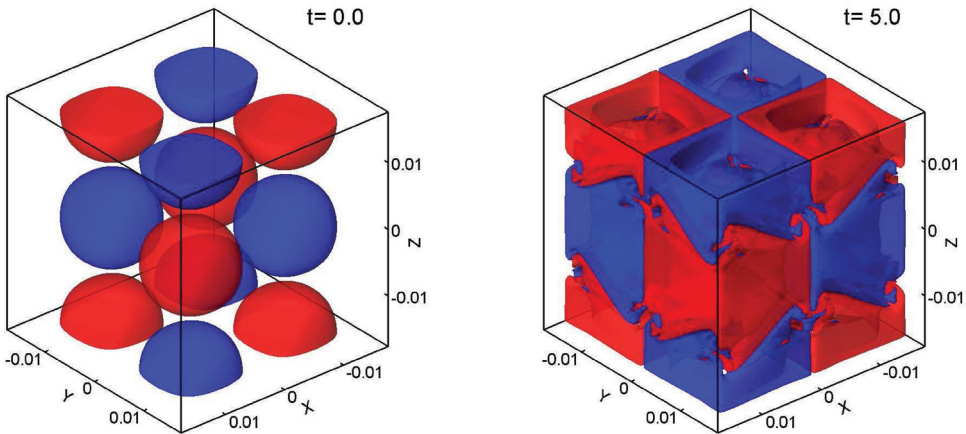


Figure 10. Evolution of iso-surfaces of z -component of vorticity for $Re = 1600$, $t = 0.0$, and $t = 5.0$.

[5], obtained by Fergus pseudo-spectral code and discontinuous Galerkin method with 96^3 degrees of freedom. The number of computational points in QGD algorithm is 64^3 and 128^3 , both with the coefficient in regularisation parameter $\alpha = 0.1$.

The good agreement with the reference data is clearly seen for the grid with 128^3 points.

7. Computational results for $Re = 1600$

In Figures 10–12, we show the iso-surfaces of the z -component of the dimensionless vorticity of the velocity field (41). As in the previous pictures, iso-surfaces are presented for the sequence of dimensionless time moments $t = 0, 5, 10, 15, 20$ and 22.5 . The red colour corresponds to $V_z = 0.7$, the blue colour corresponds to $V_z = -0.7$. Here, the grid size is 128^3 , the space step is $h = 2.5 \times 10^{-4}$ m, $\alpha = 0.1$.

From Figures 10–12, one can see that the regular initial velocity distribution (1) (Figure 10, $t = 0$) breaks down into smaller structures. At times $t = 5$ and 10 , these small-scale structures clearly retain some of the initial anisotropy of Taylor–Green vortex, but later the flow became chaotic and a nearly isotropic-developed vortex structure is seen.

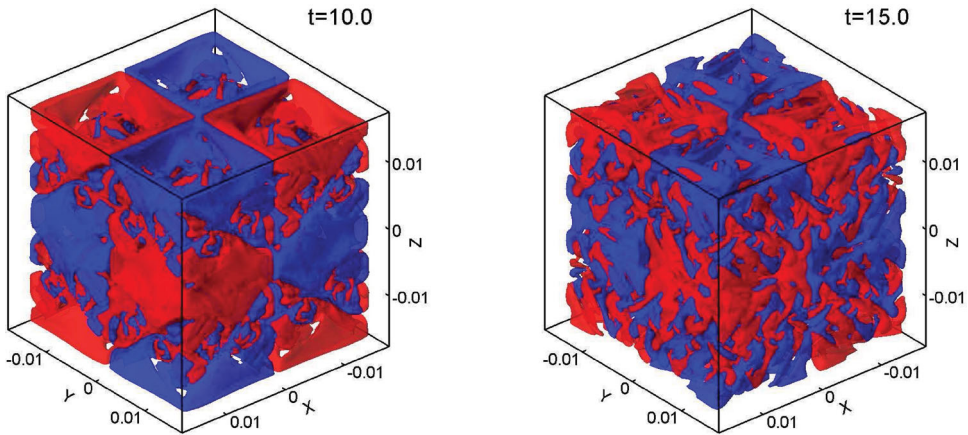


Figure 11. Evolution of iso-surfaces of z -component of vorticity for $Re = 1600$, $t = 10.0$, and $t = 15.0$.

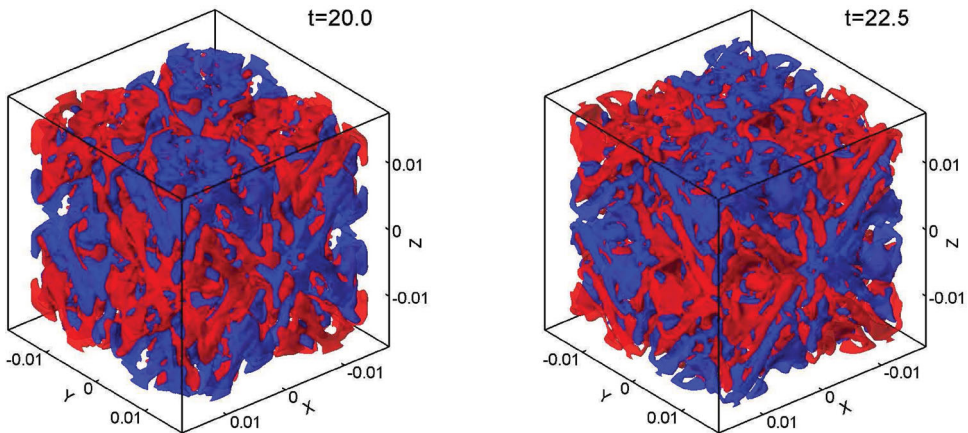


Figure 12. Evolution of iso-surfaces of z -component of vorticity for $Re = 1600$, $t = 20.0$, and $t = 22.5$.

From this moment, the flow may be interpreted as turbulent. At further times, the isotropic turbulence dies out due to viscosity. These features of the flow evolution correspond perfectly to the Taylor–Green vortex evolution presented in [1] for $Re \geq 500$, in [3] for $Re = 1600$ and in [6] for $Re = 1500$.

Figure 13 (left) shows the temporal evolution of the decaying kinetic energy E_{kin} averaged over the calculation domain V_0 (42). The solid line corresponds to our calculations with the number of grid points equal to 64^3 and 128^3 , and space steps equal to $h = 5 \times 10^{-4}$ m and $h = 2.5 \times 10^{-4}$ m, correspondingly with $\alpha = 0.1$. The dashed line shows the reference DNS data from [3] and is presented as a data file in [4], obtained by the pseudo-spectral method, and different variants of the discontinuous Galerkin method were used. Figure 13 (right) shows the temporal evolution of the dissipation rate ϵ . Both figures show that the evolutions of kinetic energy and dissipation rate obtained for 128^3 are in a quite good agreement with the reference results [3] and [4].

The Taylor–Green vortex simulations using the DNS approach are presented in a number of papers (e.g. [1, 3–6]). In particular, in [6], calculations were performed for $Re = 1500$ in

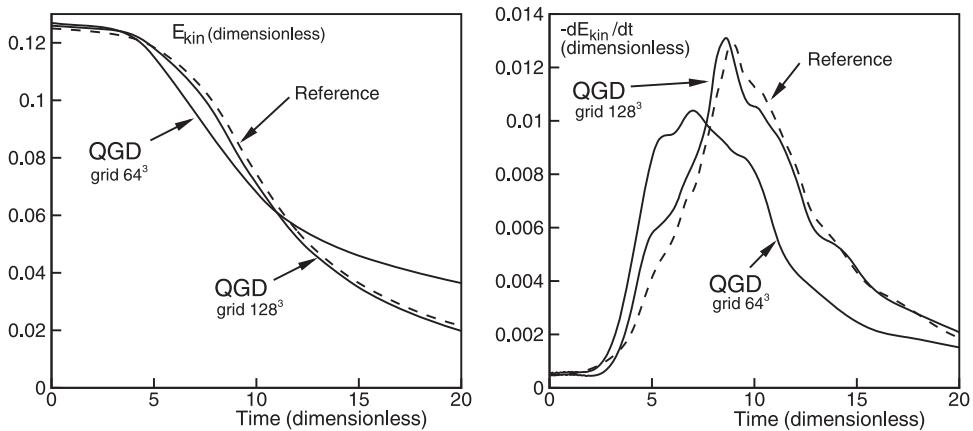


Figure 13. Time-evolution of kinetic energy E_{kin} and dissipation rate ϵ for $\text{Re} = 1600$.

a grid with 256^3 nodes using high-order methods for space and time approximations. In [6], it is pointed out that DNS simulation for $\text{Re} = 1500$ is expected to be well resolved only if the number of grid nodes is at least equal to 242^3 for uniform Cartesian computational grids. In this case, Brachet et al. [1] estimated the error of the DNS simulations of the order of only a few percent. For higher Reynolds numbers, the necessary number of grid points must be increased accordingly with the relation $N^3 \sim \text{Re}^2$ in order to obtain numerically the Kolmogorov–Obukhov dissipation cascade.

Time evolutions obtained by QGD method for 128^3 nodes are in a very good agreement with results of DNS simulations of [1] and [6] obtained for 256^3 nodes.

The LES approach allows to decrease the number of computational nodes compared with DNS methods. The results of the flow simulation for $\text{Re} = 1500$ by LES method implying the Smagorinsky filtering model for 64^3 computational nodes are demonstrated in [6]. Here the dynamic variant of the Smagorinsky model was used, in which the magnitude of the subgrid dissipation is automatically adapted according to the resolved scales in the flow. In these calculations, the maximum dissipation rate is equal to ~ 0.006 (see Figure 8.9 from [6]). The QGD algorithm for 64^3 grid gives the maximum dissipation rate ~ 0.01 , while the reference value is ~ 0.012 (see Figure 13, right). Therefore, for the Taylor–Green vortex flow under consideration, the LES model seems to be more dissipative and less accurate than QGD equations.

Influence of the computational parameters

Solution dependence from the space step h is seen from Figure 13 for $\alpha = 0.1$. Increasing of space step leads to relative smoothing of the evolution lines and displaces the maximum of the dissipation rate $\epsilon(t)$ towards smaller time. Therefore, the increasing of the step looks like the decreasing of the Reynolds number.

The convergence of the numerical solution for turbulent flow simulations is a more complex problem than for laminar cases. For laminar flows, the decreasing of space step and α proportionally increase the accuracy of the flow pattern. For turbulent flows, decreasing of h allows to resolve the smaller vortex structures, not visible on the coarse grid. This can bring some new features to the numerical solution and results in the nonlinear effects

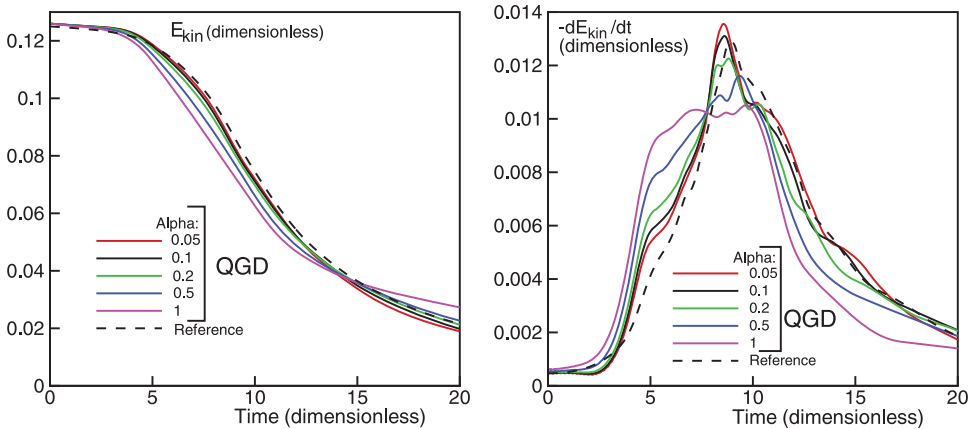


Figure 14. α -convergence of kinetic energy E_{kin} (left) and dissipation rate ϵ (right) for $\text{Re} = 1600$.

in convergence process. For turbulent flow simulation, the optimal value of the tuning parameter α may be related with the grid step and Reynolds number.

The QGD numerical algorithm presented here has only one tuning parameter, namely, α -value involved in Equation (35). The influence of α -coefficient on the computational results for grid with 128^3 points is shown in Figure 14. Increasing α from 0.05 to 1 smoothes the curves for E_{kin} and ϵ , and changes the form of the maximum dissipation rate ϵ -line. A similar effect is observed when decreasing the number of space points in the computational domain: $\alpha = 1$ for 128^3 points is similar to $\alpha = 0.1$ for 64^3 points (see Figure 13, right).

The optimal value of the smoothing parameter τ (35), for $\text{Re} = 1600$ with 128^3 grid resolution, is obtained for $\alpha = 0.1$.

Energy spectrum

The maximum value of the dissipation rate determines the zone of the laminar–turbulent transition and the formation of the classical Kolmogorov–Obukhov–5/3 scaling.

The spectral density profile $E(k)$ of kinetic energy for $\text{Re} = 1600$ is demonstrated in Figure 15. Here the Kolmogorov–Obukhov law in spectral form $E(k) \sim k^{-5/3}$ is shown for the comparison.

As in [6], the energy spectrum is calculated at time $t = 8.5$, when the ϵ -profile reaches its maximum value (see Figure 13, right). The results obtained for two computational grids with 64^3 and 128^3 points are shown. Both curves are rather similar, which proves the convergence of the numerical solution with grid refinement. The slope of the spectra approximates correctly the Kolmogorov–Obukhov law for both computational grids that show an inertial range behaviour of the flow. Increasing the number of grid points makes the curve more smooth and close to the line with $-5/3$ slope.

The obtained spectra profiles are very similar to results for $\text{Re} = 1600$, shown in Figure 4 from [5], and also to the spectra line obtained for $\text{Re} = 1500$, presented in Figure 8.3 from [6].

The algorithm of a spectral density calculation is described in detail in [34]. Here a cubic computational domain is used, and Fourier coefficients are calculated as

$$a_x^{lmn} = 8 \sum_{k=0}^{N+1} \sum_{j=0}^{N+1} \sum_{i=0}^{N+1} C_i C_j C_k \left(\frac{\rho_{ijk}}{2} \right)^{1/2} u_{xijk} \cos\left(\frac{l\pi i}{N+1} \right) \cos\left(\frac{m\pi j}{N+1} \right) \cos\left(\frac{n\pi k}{N+1} \right),$$

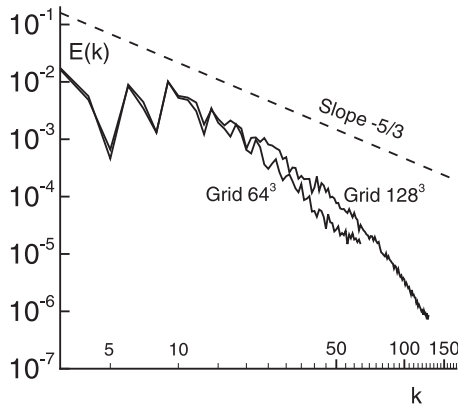


Figure 15. Spectrum of kinetic energy $E(k)$ for $Re = 1600$.

where

$$C_i = 1/2 \quad \text{for } i = 0 \quad \text{and } i = N + 1,$$

else $C_i = 1$. Here $l, m, n = [0, N]$. The values of C_j and C_k are determined analogously. In the same way, we calculate Fourier coefficients a_y^{lmn} and a_z^{lmn} .

Let us introduce

$$a^{lmn} = C_l C_m C_n ((a_x^{lmn})^2 + (a_y^{lmn})^2 + (a_z^{lmn})^2),$$

where

$$C_l = 1/2 \quad \text{for } l = 0, \quad \text{else } C_l = 1,$$

the same for C_m and C_n , $l, m, n = [0, N]$.

We determine the spectral density $E(k)$ in the following form:

$$E(k) = (N + 1)^{-6} \sum_{lmn} a^{lmn}, \quad \text{with } k - 1/2 \leq (l^2 + m^2 + n^2) < k + 1/2. \quad (43)$$

Here $0 \leq k \leq k_{max}$, where $k_{max} = N$.

The Parseval's identity, in the form

$$\int_0^{k_{max}+1} E(k) \approx \frac{1}{V_0} \int_{V_0} \frac{1}{2} \rho (u_x^2 + u_y^2 + u_z^2) dx dy dz, \quad (44)$$

is used to estimate the accuracy of the calculations. In the numerical integration, the trapezoidal rule is employed. The relative error of the numerical validation of Equation (44) has the order of $\sim 10^{-3}$.

8. Additional remarks

In the numerical simulation of turbulence, the conservation of the flow symmetry is important, because some invariants such as helicity (in 3D) and enstrophy (in 2D) are fundamentally related to the symmetry of the flow. Helicity expresses the correlation between the velocity and its curl, and it is conserved as good as a numerical scheme conserves mirror symmetry [36]. The better symmetry properties of differential operators are reproduced by finite-difference approximation, the better accuracy of the smallest scales of motion could be achieved, since the behaviour of turbulent flow on small scales is a result of a delicate balance between convective transport and diffusive dissipation [37]. In QGD calculations, the symmetry of the numerical solution is provided by the symmetrical construction of the numerical scheme that uses only the central-difference space approximations.

In order to prove the symmetry of the QGD numerical solution, all our calculations are performed in the whole computational domain. Figure 16 presents the streamlines and vorticity contours V_z in the plane $z = 0.008$ m for $Re = 1600$ (left) and $Re = 100$ (right) for $t = 20$. A developed vortex flow pattern is seen for $Re = 1600$, while for $Re = 100$, no small vortex structures are visible. Moreover, for $Re = 1600$, the level of vorticity V_z is significantly higher than for $Re = 100$. Figure 16 also demonstrates the symmetry of the numerical solution with respect to point $x = 0, y = 0$, that corresponds to the symmetry of the initial condition (1). For example, for $Re = 1600$ in the symmetric points with coordinates $(-0.008125, -0.008125, -0.008125)$ and $(0.008125, 0.008125, 0.008125)$, the values of both z -components of the vorticity are equal to $V_z = 0.229425$. This proves the correctness and symmetry properties of the QGD numerical solution.

In order to compare the numerical results for different Reynolds numbers, Figure 17 shows the temporal dependence of the dissipation rate $\epsilon(t)$ for $Re = 100$ and 280 (laminar flow evolution) and $Re = 1600$ (laminar–turbulent transition during the decay). Here $\alpha = 0.1$, and the grid consists of 128^3 points. Reference results from [1,3,5] for incompressible flows are also shown. When increasing the initial Reynolds number of the flow, the $\epsilon(t)$ maximum moves toward larger time moments ($t_0 \sim 4.5, 6$ and 8.5 , correspondingly).

Further increasing of Reynolds number to 3000 and 5000 gives almost indistinguishable results for the ϵ -peak maximum and its position, which corresponds to the time $t_0 \sim 9$ [2,8,10]. These calculations were performed by DNS, LES and implicit LES algorithms for incompressible flows. It may be suggested that for $Re \geq 3000$, the flow is close to the viscosity-independent limit.

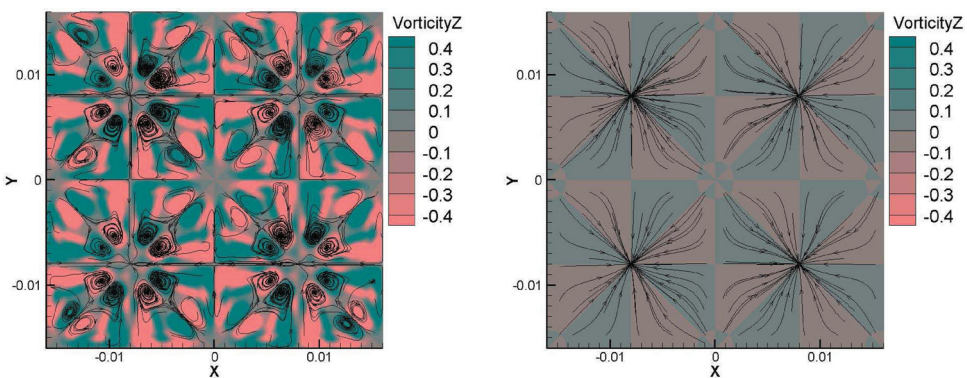


Figure 16. Symmetry of the numerical solution, $Re = 1600$ (left) and 100 (right).

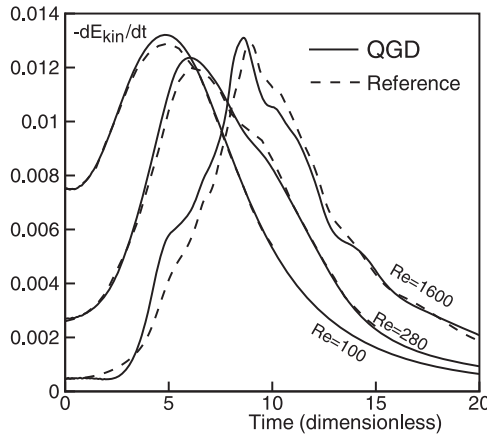


Figure 17. Comparison of dissipation rate evolution for $Re = 100, 280$ and 1600 .

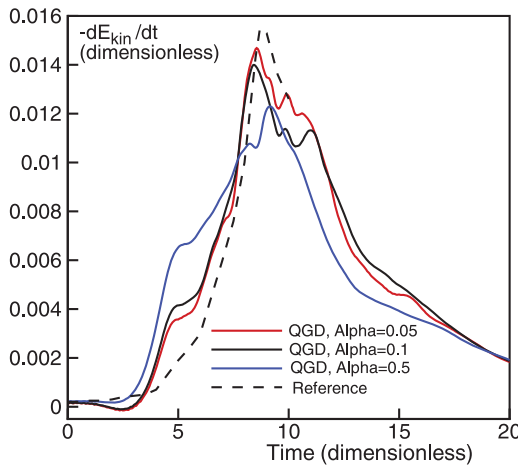


Figure 18. Dissipation rate evolution $\epsilon(t)$ for $Re = 5000$ for different values of α -coefficient.

The example of QGD calculation for $Re = 5000$ and its comparison with the reference data for ϵ value are presented in Figure 18 for $\alpha = 0.5, 0.1$ and 0.05 . Courant number is $\beta = 0.1$, and 128^3 grid points are used. In reference data [2] and [8], calculations were performed for non-dimensional time up to $t = 10$.

According to Figure 18, the optimal QGD result is archived for $\alpha = 0.05$. The differences with the reference data near the maximum value of ϵ may be explained by the fact that QGD equations describe a viscous compressible gas with kinetic and internal energy exchange. The contribution of the compressibility effects can be estimated by the pressure dilatation in the form proposed in [4,5]:

$$\epsilon_3 = -\frac{L}{\rho U_0^3 V_0} \int_{V_0} p \left(\frac{\partial u_x}{\partial x} + \frac{\partial u_y}{\partial y} + \frac{\partial u_z}{\partial z} \right) dx dy dz. \tag{45}$$

The analysis of the ϵ_3 time evolution shows that it is non-zero in the time interval $5 < t < 12$. These non-zero ϵ_3 -values may affect the delicate balance of the E_{kin} near

the maximum of $-dE_{\text{kin}}/dt$ -point. The extreme values are as follows: for $\text{Re} = 280$, $\epsilon_3 = 3 \times 10^{-5}$, for $\text{Re} = 1600$, $\epsilon_3 = 5 \times 10^{-5}$ and for $\text{Re} = 5000$, $\epsilon_3 = 1.3 \times 10^{-4}$.

For $\text{Re} = 5 \times 10^4$, QGD numerical simulations were performed up to $t = 20$ using computational grids 32^3 and 64^3 with $\alpha = 0.1$ and $\beta = 0.1$ [34]. The Kolmogorov–Obukhov-5/3 scaling spectra were obtained for $t > 9$.

9. Conclusions

In the paper, we obtain QGD equations by temporal averaging of Navier–Stokes equation system. In the previous investigations, τ -terms, which differ from the QGD system from Navier–Stokes equations, were used as effective strongly nonlinear regularisers. It gives opportunity to develop a simple finite-volume numerical algorithm for a wide range of non-stationary gas-dynamic flow calculations, namely, supersonic gas flows with strong shock waves.

Here, for the first time, the QGD algorithm is examined for simulation of laminar–turbulent transition in Taylor–Green flow. It was shown that QGD equations describe uniformly laminar and turbulent regimes including the transition to turbulence for viscous compressible gas-dynamic flows.

For laminar flows, τ -terms in QGD system work as a nonlinear adaptive dissipation and provide a monotone convergence of the numerical solution with decreasing of the space step. For turbulent flows, τ -terms act as a new variant of subgrid dissipation that smoothes the details of the unresolved scales. The quality of the numerical solution for turbulent flows may be improved by adjusting the tuning parameter α depending on Reynolds number and space step.

The numerical algorithm used to solve the QGD system consists of a central-difference approximation of the second order for all space derivatives, including convective terms, and a first-order forward-difference approximation in time. This explicit-in-time algorithm is simple for coding, and relatively cheap by computational cost, because it requires no Riemann solvers or additional monotonisation procedures. The QGD algorithm is well suited to parallel implementations.

The presented results show the perspectives of the QGD equation system in description and numerical simulations of laminar–turbulent compressible heat-conducting gas flows for subsonic and supersonic regimes.

Acknowledgements

Authors are thankful to Ivan Fedion, who has put our attention to the Taylor–Green problem, and to M.L. Shur and M.H. Streletes for the fruitful discussions of the LES methods.

Funding

The work was supported by Russian Foundation for Basic Research [grant number 13-01-00703-a].

References

- [1] M. Brachet, D. Meiron, S. Orszag, B. Nickel, R. Morf, and U. Frisch, *Small-scale structure of the Taylor–Green vortex*, J. Fluid Mech. 130 (1983), pp. 411–452.
- [2] M.E. Brachet, *Direct simulation of three-dimensional turbulence in Taylor–Green vortex*, Fluid Dyn. Res. 8 (1991), pp. 1–8.

- [3] W.M. van Rees, A. Leonard, D.I. Pullin, and P. Koumoutsakosa, *A comparison of vortex and pseudo-spectral methods for the simulation of periodic vortical flows at high Reynolds numbers*, J. Comput. Phys. 230 (2011), pp. 2794–2805.
- [4] German Aerospace Center. Available at <http://www.dlr.de/as/>
- [5] J.B. Chapelier, M. De La Llave Plata, F. Renac, and E. Martin, *Final Abstract for ONERA Taylor-Green DG Participation*, Proceedings of 1st International Workshop on High-Order CFD Methods at the 50th AIAA Aerospace Sciences Meeting, January 7–8, Nashville, TN, 2012.
- [6] D. Fauconnier, *Development of a dynamic finite difference method for large-eddy simulation*, Ph.D. thesis, Ghent University, 2008. ISBN 978-90-8578-235-3. NUR 978,928. Wettelijk depot: D/2008/10.500/55.
- [7] E. Garnier, M. Mossi, P. Sagaut, P. Comte, and M. Deville, *On the use of shock-capturing schemes for large-eddy simulation*, J. Comput. Phys. 153 (1999), pp. 273–311.
- [8] D. Drikakis, C. Fureby, F. Grinstein, and D. Youngs, *Simulation of transition and turbulence decay in the Taylor–Green vortex*, J. Turbul. 8 (20) (2007). DOI: 10.1080/14685240701250289.
- [9] A.J. Wachtor, F.F. Grinstein, C.R. DeVore, J.R. Ristorcelli, and L.G. Margolin, *Implicit large-eddy simulation of passive scalar mixing in statistically stationary isotropic turbulence*, Phys. Fluids 25 (2013), 025101-1–025101-19.
- [10] F.F. Grinstein, L.G. Margolin, and W.J. Rider, *Implicit Large Eddy Simulation*, Cambridge University Press, Cambridge, UK, 2007.
- [11] Yu.V. Sheretov, *Continuum Dynamics under Spatiotemporal Averaging*. SPC Regular and Chaotic Dynamics, Moscow-Izhevsk, 2009, in Russian.
- [12] B.N. Chetverushkin, *Kinetic Schemes and Quasi-Gas Dynamic System of Equations*, CIMNE, Barcelona, 2008.
- [13] T.G. Elizarova, *Quasi-Gas Dynamic Equations*, Springer, Dordrecht, 2009. ISBN 978-3-642-0029-5,
- [14] T.G. Elizarova, I.A. Graur, J.-C. Lendrand, and A. Chpoun, *Rarefied gas flow simulation based on quasi-gas dynamic equations*, AIAA J. 33 (12) (1995), pp. 2316–2324.
- [15] I.A. Graur, T.G. Elizarova, A. Ramos, G. Tejada, J.M. Fernandez, and S. Montero, *A study of shock waves in expanding flows on the basis of spectroscopic experiments and quasi-gas dynamic equations*, J. Fluid Mech. 504 (2004), pp. 239–270.
- [16] A. Chpoun, T.G. Elizarova, I.A. Graur, and J.-C. Lendrand, *Simulation of the rarefied gas flow around a perpendicular disk*, Eur. J. Mech. (B/Fluids) 24 (2005), pp. 457–467.
- [17] A.A. Zlotnik, *Linearized stability of equilibrium solutions to the quasi-gas-dynamic system of equations*, Doklady Math. 82 (2) (2010), pp. 811–815.
- [18] A.A. Zlotnik, *Quasi-gas-dynamic system of equations with general equations of state*, Doklady Math. 81 (2) (2010), pp. 312–316.
- [19] T.G. Elizarova and E.V. Shil'nikov, *Capabilities of a quasi-gas-dynamic algorithm as applied to inviscid gas flow simulation*, Comp. Math. Math. Phys. 49 (2009), pp. 532–548; *Erratum*. Comp. Math. Math. Phys. 50 (4) (2010), pp. 747–748.
- [20] E. Johnsen, J. Larsson, A.V. Bhagatwala, W.H. Cabot, P. Moin, B.J. Olson, P.S. Rawat, S.K. Shankar, B. Sjogreen, H.C. Yee, X. Zhong, and S.K. Lele, *Assessment of high-resolution methods for numerical simulations of compressible turbulence with shock waves*, J. Comput. Phys. 229 (2010), pp. 1213–1237.
- [21] T.G. Elizarova, P.N. Nikolskii, and J.C. Lengrand, *A New Variant of Subgrid Dissipation for LES Method and Simulation of Laminar-Turbulent Transition in Subsonic Gas Flows*, in *Advances in Hybrid RANS-LES Modelling*, Shia-Hui Peng and Werner Haase, eds., Springer-Verlag, Berlin, 2008, pp. 289–298.
- [22] T.G. Elizarova and V.V. Seregin, *Filtered simulation method for turbulent heat and mass transfer in gas dynamic flows*, in *Proceedings of the 6th International Symposium on Turbulence, Heat and Mass Transfer, Rome, 14–18 September*, K. Hanjalic, Y. Nagano, S. Jakirlic, eds., Begell House Inc., 2009, pp. 383–386.
- [23] T.G. Elizarova and I.A. Shirokov, *Numerical simulation of a non-stationary flow in the vicinity of a hypersonic vehicle*, Math. Model Comput. Simul. 4 (4) (2012), pp. 410–418.
- [24] T.G. Elizarova and I.A. Shirokov, *Direct simulation of laminar-turbulent transition in a viscous compressible gas layer*, Comput. Math. Model. 25 (1) (2012), pp. 27–48.
- [25] K-100 System, Keldysh Institute of Applied Mathematics RAS, Moscow; Available at <http://www.kiam.ru/MVS/resourses/k100.html>

- [26] G.A. Bird, *Molecular Gas Dynamics and the Direct Simulation of Gas Flows*, Clarendon Press, Oxford, 1998.
- [27] T.G. Elizarova and I.A. Shirokov, *Laminar and turbulent regimes of Taylor-Green vortex decay*, preprint (2013), Keldysh Institute of Applied Mathematics of Russian Academy of Science, N 63. 16 p. Available at <http://library.keldysh.ru/preprint.asp?id=2013-63>.
- [28] T.G. Elizarova, *Time averaging as an approximate technique for constructing quasi-gas-dynamic and quasi-hydrodynamic equations*, *Comput. Math. Math. Phys.* 51 (11) (2011), pp. 1973–1982.
- [29] L.G. Loitsyanskii, *Mechanics of Liquids and Gases*, Begell House, New York, 1996; Drofa, Moscow, 2003.
- [30] L.D. Landau and E.M. Lifshitz, *Fluid Mechanics*, Nauka, Moscow, 1986; Pergamon Press, Oxford, 1987.
- [31] A. Aspden, N. Nikiforakis, S. Dalziel, and J.B. Bell, *Analysis of implicit LES methods*, *Comm. App. Math. Comp. Sci.* 3 (1) (2008), pp. 103–126.
- [32] A. Zlotnik and V. Gavrilin, *On quasi-gasdynamic system of equations with general equations of state and its application*, *Math. Model. Anal.* 16 (4) (2011), pp. 509–526.
- [33] T.G. Elizarova and O.V. Bulatov, *Regularized shallow water equations and a new method of simulation of the open channel flows*, *Comput. Fluids.* 46 (1) (2011), pp. 206–211.
- [34] T.G. Elizarova and I.A. Shirokov, *Testing of the QGD algorithm by a homogeneous isotropic gas-dynamic turbulence decay*, preprint (2013), Keldysh Institute of Applied Mathematics of Russian Academy of Science, N 35. 19 p. Available at <http://library.keldysh.ru/preprint.asp?id=2013-35>.
- [35] T.G. Elizarova, A.A. Khokhlov, and Yu.V. Sheretov, *Quasi-gas-dynamic numerical algorithm for gas flow simulations*, *Int. J. Numer. Method Fluids* 56 (8) (2008), pp. 1209–1215.
- [36] A. Pouquet and P.D. Mininni, *The interplay between helicity and rotation in turbulence: implications for scaling laws and small-scale dynamics*, *Phil. Trans. R. Soc. A* 368 (2010), pp. 1635–1662.
- [37] R.W.C.P. Verstappen and A.E.P. Veldman, *Symmetry-preserving discretization of turbulent flow*, *J. Comput. Phys.* 187 (2003), pp. 343–368.